Journal of Nuclear Medicine, published on March 9, 2018 as doi:10.2967/jnumed.117.205393

^{18}F-FDG micro-PET imaging for research investigations in the *Octopus vulgaris*: applications and future directions in invertebrate neuroscience and tissue regeneration

Letizia Zullo[1]*, Ambra Buschiazzo[2], Michela Massollo[3], Mattia Riondato[4,5], Alessia Democrito[5], Cecilia Marini[2,5,6], Fabio Benfenati[1,7], Gianmario Sambuceti[2,5,6]

[1] Center for Synaptic Neuroscience and Technology, Istituto Italiano di Tecnologia, Genoa, Italy

[2] Department of Health Science, Nuclear Medicine, University of Genoa, Genoa, Italy

[3] Nuclear Medicine Unit, EO Galliera Hospital, Genoa, Italy

[4] *present address*: Nuclear Medicine Department, S. Andrea Hospital, La Spezia, Italy

[5] Nuclear medicine unit, IRCCS San Martino, Genoa, Italy

[6] Institute of Molecular Bio-imaging and Physiology (IBFM), CNR, Milan, Italy

[7] Department of Experimental Medicine, University of Genova, Genoa, Italy

* Corresponding Author: Letizia Zullo, PhD

Center for Synaptic Neuroscience and Technology, Istituto Italiano di Tecnologia,

Largo Rosanna Benzi, 10, Torre D1, 16132, Genoa, Italy

Tel: 0105558382 Fax: 0105558491

e-mail: letizia.zullo@IIT.it

ABSTRACT

This study aimed at developing a method for administration of ^{18}F-Fludeoxyglucose (^{18}F-FDG) in the common octopus and micro-positron emission tomography (micro-PET) bio-distribution assay for the characterization of glucose metabolism in body organs and regenerating tissues. **Methods**: Seven animals (two with one regenerating arm) were anesthetized with 3.7% $MgCl_2$ in artificial seawater. Each octopus was injected with 18-30 MBq of isosmotic ^{18}F-FDG by accessing the branchial heart or the anterior vena cava. After an uptake time of ~50 minutes, the animal was sacrificed, placed on a bed of a micro-PET scanner and submitted to 10 min static 3-4 bed acquisitions to visualize the entire body. To confirm the interpretation of images, internal organs of interest were collected. The level of radioactivity of each organ was counted with a γ-counter. **Results:** Micro-PET scanning documented a good ^{18}F-FDG full body distribution following vena cava administration. A high mantle mass radioactivity facing a relatively low tracer uptake in the arms was revealed. In particular, the following organs were clearly identified and measured for their uptake: brain (standardized uptake value, SUV max of 6.57±1.86), optic lobes (SUV max of 7.59±1.66) and arms (SUV max of 1.12±0.06). Interestingly, ^{18}F-FDG uptake was up to threefold higher in the regenerating arm stumps at the level of highly proliferating areas. **Conclusion**: This study represents a stepping-stone over the use of non-invasive functional techniques to address questions relevant to invertebrate neuroscience and regenerative medicine.

KEYWORDS

Octopus, ^{18}F-FDG, micro-PET, functional imaging, regeneration

INTRODUCTION

Cephalopods are among the most intelligent invertebrates and they represent a class of highly specialized mollusks where neural and morphological novelties emerged together (*1,2*). Their behavioral capabilities and highly evolved neural system have prompted their recent inclusion in the list of species undergoing European Union ethical regulation (*3-5*). In this perspective, there is an increasing need for minimally invasive experimental approaches that, by reducing the impact of surgery, will allow functional investigation on behavior, neurophysiology and body function of live cephalopods. Octopuses are easily maintaining and handling animals and they can have an appropriate size for a canonical high-resolution micro-positron emission tomography (micro-PET) system.

^{18}F-Fludeoxyglucose PET (^{18}F-FDG PET) is a widely used tool for *in vivo* study of oncological, cardiovascular, and neurological disorders, as well as for study of cerebral glucose metabolism (*6-9*). Due to the interest in developing novel therapeutic strategies in the field of bone and cardiovascular muscle repair, this technique is also becoming relevant to studies of bone regeneration and cardiac remodeling (repair and regeneration), because it allows following tissue regeneration through non-invasive measurements of metabolic processes (*10-12*).

Animals might use a variety of different strategies of repair and regeneration leading to the partial or full restoration of the missed function. Given the limited regeneration capacity of mammalians, these processes have been historically studied in a wide variety of vertebrates and invertebrates. The final aim is the assessment of common regeneration principles for the development of new therapeutic approaches in regenerative medicine.

Due to its great regenerative potential, the cephalopod mollusks *Octopus vulgaris* represents a viable alternative to vertebrate regeneration models. Cephalopods can regenerate missing or injured structures such as the shell, the appendages (arms and tentacles), the cornea, peripheral nerves and brain centers

(for a review, see (*13*)). In particular, Octopuses have a complex arm structure and physiology (*14-16*) that shares similarities in early arm development and regeneration to vertebrate models (*13,17,18*). This makes it an ideal model for studying limb regeneration and finding conserved pathways that might be triggered in various animal species (including mammals) to induce regeneration of injured tissue.

In this study, we developed a protocol of injection of ^{18}F-FDG radiolabeled solution accessing the venous system of *Octopus vulgaris* and then tested the use a common ^{18}F-FDG micro-PET technique, employed in higher vertebrates' examination, to investigate glucose metabolism in the octopus internal organs and regenerating limbs. Blood circulation in coleoids is based upon a completely closed and highly efficient circulatory system composed by a tri-partite heart with a system of mostly contractile vessels that distribute the blood throughout the body (*19*). Relevant to our study, the presence of contractile blood vessels within the arms (*20*) assures a good rate of blood flow even at far distances from the heart and in the presence of high internal pressure, which often can occur in soft-bodied animals. We therefore evaluated the bio-distribution of ^{18}F-FDG along the arms and assessed the occurrence of an increase in metabolic rate at the regenerating arm tips.

MATERIALS AND METHODS

The study and all procedures involving experimental animals were approved by the Institutional Review Board and by the Italian Ministry of Health (authorization n. 1111/2016-PR). Our research conformed to the ethical principles of the three Rs (replacement, reduction and refinement) and of minimizing of animal suffering, following the Directive 2010/63/EU (Italian D. Lgs. n. 26/2014) and the guidelines from Fiorito et al. (*5*).

Animal treatment. Specimens of *Octopus vulgaris* of either sex were collected from the Liguria coast during the spring/summer period 2013 and 2017 and placed in 80x50x45 cm marine aquaria. The tanks were filled with artificial seawater (ASW) and kept at a temperature of 18 °C at 12 h light/dark cycle. Water cleaning and oxygenation were assured by a pump-filter and aeration system that continuously circulated the water through biological filters. All relevant chemo/physical water parameters were constantly checked to prevent the occurrence of unhealthy or stress conditions. Animals were left to adapt to captivity for at least 10 days. The experimental animals were selected on the basis of the following criteria: healthy shape (all the arms and body parts had to be intact, the animal showed normal reflexes and voluntary movements such as arm extension, walking, etc.), regular eating and motivation to attack a prey (*4,5,21-23*).

Seven animals weighing 150-450 g were used in the two experimental protocols, two of them were also employed in the regeneration study, as described below.

Regeneration Protocol. Two animals of 150g (Animal 1) and 182 g (Animal 2) underwent surgical amputation of the arm tip to induce the process of arm regeneration. In order to do so, each animal was anesthetized in 2% ethanol in ASW for about 5 min (*5,24,25*) and until a clear change in body patterns and posture, cessation of ventilation, unresponsiveness to external stimuli and loss of righting reflex confirmed that the cephalopod underwent the physiological process of anesthesia. Ethanol was preferred for this operation given that anesthesia duration and recovering time are both fast (5). A portion not exceeding 10% of the total arm length was cut from the first left arm (L1) from each animal with fine scissors on a transverse plane and was then allowed regenerating for 11 (Animal 1) and 33 days (Animal 2). Following surgery, the animals were placed back in their experimental tank where they slowly (about 2–5 min) recovered from anesthesia. The animals did not display behavioral modification nor signs of

distress or suffering after the operation, and the amputated arm regenerated as in the natural environment (*4,5,25-27*).

Bio-distribution analysis. Animals were anesthetized by adding a solution of $MgCl_2$ to the final concentration of 3.7% in ASW. Animals received a single dose of radiotracer solution (200-300 µl of isosmotic ^{18}F-FDG, 18-30MBq) while maintained under anesthesia and then immediately transferred to the fresh ASW container in order to prevent branchial ventilation and heartbeat to stop and to facilitate the radiotracer distribution along the body. Animals were divided into two experimental groups. The first one composed of 3 animals (L-BH animals) receiving a single injection of the radionuclide solution through the left branchial heart and used for microPET scanning and γ-counting. The second one composed of two animals (VC animals) injected through the anterior vena cava and two animals injected through the vena cava and carrying one regenerating limb. Both administration routes are upstream the redistribution of the blood to the organs (Fig. 1) and have been described in (5). Following Best practice protocols, an uptake time of 50 minute was employed in order to maximize the chances of accumulation of radiotracers overall the animal body. Indeed, following the standard protocol for humans and other studied models, all organs are assumed to reach a complete FDG uptake at this time (*8,28*). Animals were then brought to terminal anesthesia by adding an overdose of $MgCl_2$ to the same ASW where the animal was kept after injection. In this case, $MgCl_2$ has to be preferred as it produce at the same time animal terminal death and a complete muscle relaxation, thus avoiding spontaneous reflex movements that can compromise the goodness of scanning.

The animals were then removed from the water, placed on a bed of a micro-PET scanner (Albira, Bruker, US) and submitted to a 10-min static 3-4 bed acquisitions (depending on the animal total length). The animal was positioned so that its mantle, brain and eyes were scanned during the first and second bed acquisition. PET data were reconstructed using a maximal likelihood expectation maximization method

(MLEM). An experienced observer, unaware of the experimental type of the analyzed octopuses, identified a volume of interest (VOI) in the studied organs to measure standardized uptake value (SUV). Measures were expressed as SUV_{max} ± SE. Internal organs of interest, hemolymph (the cephalopod blood), brain and muscle portions were sampled, blotted dry, weighted and their radioactivity was counted in a Cobra II γ-counter (Packard Bell) with energy window set at 511 KeV. Decay corrected activity rate (in counts per minute, cpm) was always performed considering the time interleaved between counting and injection. Counts were expressed as means (± SE) percentages of the injected dose per gram of tissue (%ID/g).

Graphics program

All figures were prepared with Adobe Photoshop CS5 version12.0.

Statistical Analysis. Statistical analysis was performed using SigmaPlot 13.0 (Systat Software, Inc.). The distribution of the data was first assessed with a normality test (Shapiro-Wilk). Differences among dataset were verified by t-test and ANOVA. Kruskal-Wallis and Mann-Whitney Rank Sum test was used in non-parametric tests. P values <0.05 were considered significant.

RESULTS

Bio-distribution studies

The level of radioactivity accumulated by various organs in L-BH animals was measured at the γ-counter (%ID/g ± SE) and with micro-PET (SUV_{max} ± SE) and data were compared to assess the correlation between micro-PET whole body and γ-counting of the target organs (see below).

γ-counting

Activity at non-target sites was also measured to disclose possible signs of contaminations. Octopus beak was chosen as a non-target organ as it is mostly composed of acellular chitin components and therefore it does not represent a good site of radiotracer accumulation. Activity at this level was low (Fig. 2; 0.19±0.14 %ID/g; n=3). Uptake in the samples of hemolymph was from ~0.4 to 3 %ID/g (n=3) and that found in the excreted solution (sampled from the water bath where the animal was held after injection and then brought to terminal anesthesia) was very low (0.013±0.004%ID/g; n=9).

After L-BH injections, activity of the left branchial heart and gill were very high (respectively 11.72±2.05%ID/g and 21.08±3.40%ID/g; n=3). The organs with high metabolic rates, such as the brain and optic lobes showed a good uptake level (2.04±0.28 and 5.37±0.34 %ID/g, respectively; n=3). Several organs such as the stomach, intestine and hepatopancreas displayed a high and very variable level of accumulation of the tracer probably due to their digestion related functions (from ~1 up to 12 %ID/g; n=3). Low uptakes were measured in muscle samples (0.54±0.68 %ID/g; n=3). Organs directly receiving the blood from the injected heart, such as gill and optic lobe, showed the highest uptake (from ~5 to 21 %ID/g; n=3) with a marked increase in the side of the body injection (Fig. 2; *t*-test, $P<0.05$ n=3). Organs farther from the administration site did not show signs of lateralization (Fig. 2, ANOVA, $P>0.05$; n=3).

Since this lateralization might have prevented a good and even redistribution of the radiotracer to the two body sides, in the second set of experiments and in regeneration experiments the radiotracer was injected through the VC located medially in the body and upstream the branchial hearts. This vena is easy to access and the intrinsic elasticity of the vein (see Introduction) should help to minimize radiotracer leakage from the injection point.

microPET scanning

We performed a measure of the radioactivity accumulated in L-BH and VC animals with microPET scanning. As expected, a marked accumulation of radioactivity at the branchial heart is evident in L-BH animals (Fig.3A,C) but not in VC animals (Fig. 3C,D). Organs with high metabolic activity such as central brain, optic lobes and various internal organs were clearly distinguishable for their high SUV values in both experimental group (Fig.3 A,B). To quantify this data we perfomed SUV analysis of the organs easily identifiable within the microPET volume image with very low scope for error.

We found that in L-BH animals radioactivity at the injected heart is the highest and is immediately followed by activity in corresponding gill while the signal drops markedly down in the remaining organs (Fig. 3E). This is especially evident when comparing SUV values in VC and L-BH groups in which a generalized lower body uptake can be observed (Fig.3E). Hence, a considerable amount of radiotracer residues seems to accumulate in the injected heart, thus affecting the radioactivity measured at the level of both the branchial heart and corresponding gill.

In details, after L-BH administration, the brain (Fig. 3A, yellow arrows; Fig. 3E, SUV_{max} 2.49$\pm$1.32 n=3) and optic lobes (Fig. 3A, black arrowheads; Fig. 3E, SUV max 3.32±1.83; n=3) showed high SUV. Relative to the non-neural areas, a low uptake was measured at the level of the arms (Fig. 3A, red arrowheads; Fig. 3E, SUV_{max} 0.44±0.64; n=3).

Animals receiving VC administration showed similarly high SUV values in brain (Fig. 3B yellow arrows; Fig. 3E, SUV_{max} 6.57±1.86; n=2) and optic lobes (Fig. 3B black arrowheads; Fig. 3E, SUV max

7.59±1.66; n=2) and low SUV at the level of the arms (Fig. 3B, red arrowheads; Fig. 3E, VC SUV_{max} 1.12±0.06; n=2). The low level of arm uptake can be explained considering that muscle energetics mostly depend on glycogen catabolism, while glycolysis only accounts for a small part of the muscle metabolic demand.

To make a clearer estimate of the overall body uptake, we plotted the distribution of SUV_{max} of the selected organs (excluding left branchial heart and gill, that might have been directly affected by residuals of the injected radionuclide) in the in the two experimental groups. We compared these values and found that VC animals have a significantly higher uptake that L-BH (Figure 4A Mann-Whitney Rank Sum Test, $P<0.05$; n=5).

We next wanted to address the question of whether the injection method could also produce a lateralization effect of radiotracer diffusion and uptake. In order to do so, left and right SUV components were calculated. Interestingly, in VC animals the activity was evenly distributed at the two body sides while in L-BH animals a significant accumulation in the left side was revealed (Fig. 4B, *t*-test, $P<0.01$; n=5). In the latter, the level of accumulation in the left side was also significantly higher than in left and right sides of VC animals (Fig. 4B, *t*-test, $P<0.05$; n=5).

Overall, our data indicate that following VC injection the radioactive solution efficiently circulates throughout the body, reaches all organs and is efficiently retained by those with a higher metabolic rate.

^{18}F-FDG uptake in regenerating arm

Two animals, respectively at 11 (Animal 1) and 33 (Animal 2) days of regeneration, underwent the same procedure described above; regenerating and non-regenerating arm portions were measured for their ^{18}F-FDG uptake with micro-PET scanning. Activity in non-regenerating arms was higher at the central arm axes. This can be due to the presence of a massive population of neuronal cells forming the arm peripheral nervous system and located right at the center of the arm. As for other neural structure, neurons of the

PNS consume a large amount of glucose to sustain their function and thus show a high FDG uptake. The activity in the regenerating arm stump was measured at two different locations, at its base and tip. These values were compared to the activity of non regenerating arms in the same animal. Activity at the base of the stump was equal to that of a corresponding region in non-regenerating arms while a 60% (Animal 1) and 20% (Animal 2) increase in ^{18}F-FDG uptake was revealed at the arm tip. We then measured the proximo-distal extension of the high metabolic areas and found it to cover a region from ~4-6 mm from the arm tip (Fig. 5A, B; n=2). At the stages of regeneration analyzed, the arm tip is populated by a different amount of intensely proliferating cells located at blastemal, nervous system and muscle level (Fig. 6; brown precipitates represent PCNA (proliferating cell nuclear antigen) staining) (*29*). In particular, at about 11-17 days of regeneration the arm tip has the highest level of cell proliferation while around 33 days of regeneration proliferation goes down although still settling above basal levels (*29*). This might account for the large variability in uptake increase observed in the two regenerating arms. Vascular components are also present but we believe that their possible contribution to the activity measured is very exiguous (Figure 6). This is supported by the following two consideration. First, when present, the vascular components reached a proximo-distal area of up to 1 mm (see Fig. 6) while high uptake values extended over 4-6 mm from the arm tip. Second, the activity of the circulating FDG in the emolymph, that could potentially influence the radioactivity of a high vascularized region and sinus, was measured right after scanning and resulted to be extremely low.

In conclusion, the high level of FDG uptake observed in the regenerating arm tips might well reflect the presence of actively dividing cells in blastema, peripheral nervous tissue and muscles characteristic of regenerating tissues.

DISCUSSION

To the best of our knowledge, this is the only study after the first 1992 investigation (*30*) where a labelled glucose analogue has been used to map the metabolic activity of body regions of a cephalopod. Several radiotracers have been employed in late ’70 studies to assess, in particular, protein synthesis in various invertebrates including cephalopods. These investigations demonstrated the reliability of radiolabeling techniques to mark metabolic active organs such as gills, hearts, liver, hepatopancreas, brain, muscle and even arm tips (*31-35*). The accumulation of radioactive compound was detected by means of liquid-scintillation counting and autoradiography. Both these methodologies suffer from their being limited to static detection and *ex-vivo* study and cannot answer questions relative to functional *in-vivo* body physiology.

Micro-PET ^{18}F-FDG techniques allows a high resolution live-scanning of high metabolically active body regions and are widely used in clinical and pre-clinical studies in a variety of different fields.

In particular, clinical imaging is an indispensable tool for characterizing damaged tissue in regenerative medicine. At present, only a few investigations take advantage of this technique to assess and follow regeneration processes; these have particular relevance for issues relative to bone regeneration and cardiac remodeling (*10,11*).

Due to the innate constrain of vertebrates in their regeneration ability, the use of alternative animal models to study regeneration has been long envisaged. Cephalopods and octopods are renowned for their high regeneration abilities and might serve as models for comparative regenerative investigations. In addition, cephalopods are endowed with a ‘vertebrate-like’ completely closed circulatory system working at high pressure, a characteristic that is unique among invertebrates and that assures a fast and efficient blood flow throughout the body (*36,37*).

As glucose metabolism in cephalopods is based upon enzymes and reactions essentially similar to that of higher animals, in this study, we assessed the use of the common ^{18}F-FDG micro-PET clinical methodology to perform full body bio-distribution assay in *Octopus vulgaris*.

Circulation in cephalopods is assured by a vascular and an aortic system, one pair of branchial hearts, each associated with the corresponding gill at the one side of the body, and one central systemic heart (Fig. 1). In addition, a system of contractile veins assures that the oxygenated blood reaches the central systemic heart that will in turn actively pump it to the rest of the body. Blood pressure and flow rate in cephalopods give a time around 120 sec for the complete circulation of total blood volume, thus allowing fast circulation of the tracer (*38*). Here, we performed a direct injection of small doses of radionuclide into the animal venous system; this resulted in a full body distribution of the radiolabeled compound. A clear lateralization of the uptake occurred following administration through the BH in organs localized immediately downstream the injection location. This might be explained by the nature and structure of the octopus branchial heart that is mainly nonmuscolar and formed by a mass of spongy and poorly associated cells. Such a conformation might prevent a rapid efflux of the radionuclide solution towards the circulatory system. Following injection through the VC, a higher level of uptake was revealed in the overall body along with the absence of lateralization. This suggests that VC administration is the only alternative to avoid radionuclide redistribution biases.

The injected dose (ID) of the radionuclide was calculated based on standard protocols used for rats of similar weight. The rationale behind our choice is based on the similarity of blood volume (around 5.8% of the animal wet weight and extracellular volume of 28%) and circulating glucose (in the order of 0.8-2 μmol/ml) between cephalopods and mammals (*39,40*). Glucose in cephalopods is an important fuel for all the organs, including muscles, but is essential for brain and heart for which oxidation of blood glucose is the main energy source. Our imaging results well reflected the expected glucose distribution and consumption in the various organs. In particular, organs with a high metabolic rate such as the brain,

optic lobes and heart have high incorporation values, while a low uptake was found in the arms (mostly muscular).

We next wanted to test the sensitivity of the ^{18}F-FDG microPET methodology to investigate differences in the metabolic activity of regenerating and non-regenerating arms. During the early stages of morphogenesis, the arm is characterized by the massive presence of highly proliferating cells largely dependent on a fast and efficient energy production through glucose metabolism (*14,17,18,29,41*). Adult fully differentiated muscles have a low growth rate at rest, a moderate activity of hexokinase and rely more on glycogen catabolism (*35,42,43*). Therefore, regenerating tissue might accumulate labelled glucose at a higher rate than other cells located in non-regenerating tissues.

Our detailed micro-PET analysis shows that the uptake values of the regenerating arms are up to threefold higher than that of control non-regenerating arms. Interestingly, a 3D reconstruction of the regenerating arms also showed that the localization of the higher metabolic areas matches that occupied by highly proliferating muscular and undifferentiated tissue, as previously described in a fine morphology investigation (*29*). The present study might provide an important step towards the functional and molecular assessment of the regeneration process in various tissues and organs, as well as the live visualization of the nervous system activity. In order to do so, animals must be repeatedly scanned to assess metabolic changes occurring in the organ of interest over time. Hence, it will be necessary to test the animal recovery from deep anesthesia under which it should be maintained for the entire scanning duration. Available data on anesthesia duration suggest this implementation to be possible in this animal species as it can be kept fully anesthetized for ~20 minutes (*5*). Moreover, animal size can be downscaled to reduce scanning time to 10-20 minutes (1 to 2 beds) and a coverage of the entire animal with 3.7% MgCl2 ASW embedded tissue coats would prevent skin and eye to dry and will help keeping the animal under a prolonged anesthesia.

Further upgrades, such as the use of a dynamic micro-PET scanning and the employment of cell-specific radiolabeled compounds can be envisaged to achieve various targets. Taken together, this will be particularly relevant in the field of behavioral neuroscience thus giving the possibility to link in vivo brain activity and behavioral traits with minimally invasive investigations.

Conclusion

The standard ^{18}F-FDG micro-PET system is a valuable tool for investigating metabolically active body regions at a single organ resolution in the cephalopod mollusk *Octopus vulgaris*. Administration of a radioactive compound through the anterior vena cava has to be preferred in bio-distribution studies and this methodology can be employed for the assessment of regenerating events occurring at various regions of the animal body. This study represents a first step toward the use of nuclear medicine imaging techniques in new emerging research areas such as neurobiology of invertebrates and animals with particular relevance in the field of regenerative medicine.

Funding. No funding was received for this study.

Conflict of interest. The authors declare that they have no conflict of interest.

Ethical approval. All applicable international, national, and/or institutional guidelines for the care and use of animals were followed. All procedures involving animals were in accordance with the ethical standards or practice of the institution at which the studies were conducted.

Acknowledgments

We thank Dr. Sara Maria Fossati and Dr. Arta Mehilli for technical help and animal maintenance.

REFERENCES

1. Albertin CB, Simakov O, Mitros T, et al. The octopus genome and the evolution of cephalopod neural and morphological novelties. *Nature.* 2015;524:220-224.

2. Lee PN, Callaerts P, de Couet HG, Martindale MQ. Cephalopod Hox genes and the origin of morphological novelties. *Nature.* 2003;424:1061-1065.

3. Berry A, Vitale A, Carere C, Alleva E. EU guidelines for the care and welfare of an "exceptional invertebrate class" in scientific research. Commentary. *Ann Ist Super Sanita.* 2015;51:267-269.

4. Fiorito G, Affuso A, Anderson DB, et al. Cephalopods in neuroscience: regulations, research and the 3Rs. *Invert Neurosci.* 2014;14:13-36.

5. Fiorito G, Affuso A, Basil J, et al. Guidelines for the Care and Welfare of Cephalopods in Research -A consensus based on an initiative by CephRes, FELASA and the Boyd Group. *Lab Anim.* 2015;49:1-90.

6. Maya-Vetencourt JF, Ghezzi D, Antognazza MR, et al. A fully organic retinal prosthesis restores vision in a rat model of degenerative blindness. *Nat Mater.* 2017;16:681-689.

7. Phelps ME. Positron computed tomography studies of cerebral glucose metabolism in man: theory and application in nuclear medicine. *Semin Nucl Med.* 1981;11:32-49.

8. Sokoloff L, Reivich M, Kennedy C, et al. The [14C]deoxyglucose method for the measurement of local cerebral glucose utilization: theory, procedure, and normal values in the conscious and anesthetized albino rat. *J Neurochem.* 1977;28:897-916.

9. Marini C, Salani B, Massollo M, et al. Direct inhibition of hexokinase activity by metformin at least partially impairs glucose metabolism and tumor growth in experimental breast cancer. *Cell Cycle.* 2013;12:3490-3499.

10. Naumova AV, Modo M, Moore A, et al. Clinical imaging in regenerative medicine. *Nat Biotech.* 2014;32:804-818.

11. Annibali S, Bellavia D, Ottolenghi L, et al. Micro-CT and PET analysis of bone regeneration induced by biodegradable scaffolds as carriers for dental pulp stem cells in a rat model of calvarial "critical size" defect: Preliminary data. *J Biomed Mater Res B Appl Biomater.* 2014;102:815-825.

12. Sommese L, Zullo A, Schiano C, et al. Possible Muscle Repair in the Human Cardiovascular System. *Stem Cell Rev.* 2017;13:170-191.

13. Zullo L, Fossati SM, Imperadore P, Nodl MT. Molecular Determinants of Cephalopod Muscles and Their Implication in Muscle Regeneration. *Front Cell Dev Biol.* 2017;5:53.

14. Fossati SM, Benfenati F, Zullo L. Morphological characterization of the Octopus vulgaris arm. *Vie et Milieu.* 2011;61:197-201.

15. Zullo L, Fossati SM, Benfenati F. Transmission of sensory responses in the peripheral nervous system of the arm of Octopus vulgaris. *Vie et Milieu.* 2011;61:197-201.

16. Kier WM. The Musculature of Coleoid Cephalopod Arms and Tentacles. *Front Cell Dev Biol.* 2016;4:10.

17. Fossati SM, Candiani S, Nodl MT, et al. Identification and Expression of Acetylcholinesterase in Octopus vulgaris Arm Development and Regeneration: a Conserved Role for ACHE? *Mol Neurobiol.* 2015;52:45-56.

18. Nodl MT, Fossati SM, Domingues P, Sanchez FJ, Zullo L. The making of an octopus arm. *Evodevo.* 2015;6:19.

19. Wells MJ. Circulation in Cephalopods. In: Saleuddind ASM, Wilbur KM, eds. *The Mollusca.* Vol 5, Physiology, Part 2. New York: Academic press; 1983.

20. Mislin H, Kauffmann M. Der aktive Gefässpuls in der Arm-Schirmhaut der Cephalopoden. *Revue suisse Zool.* 1948;55:267–271.

21. Piero Amodio, Paul Andrews, Marinella Salemme, Giovanna Ponte, Fiorito G. The Use of Artificial Crabs for Testing Predatory Behavior and Health in the Octopus *ALTEX.* 2014;31:494-499.

22. Marini G, De Sio F, Ponte G, Fiorito G. Behavioral Analysis of Learning and Memory in Cephalopods. In: Byrne JH, ed. *Reference Module in Neuroscience and Biobehavioral Psychology*. Amsterdam: Academic Press, Elsevier; 2017:441–462.

23. Maldonado H. The positive learning process in Octopus vulgaris. *Zeitschrift für vergleichende Physiologie.* 1963; 47:191–214.

24. Andrews PLR, Tansey EM. The effects of some anesthetic agents in Octopus vulgaris. *Comp Biochem Physiol.* 1981;70C:241–247.

25. Crook RJ, Walters ET. Nociceptive behavior and physiology of molluscs: animal welfare implications. *ILAR J.* 2011;52:185-195.

26. Hague T, Florini M, Andrews PLR. Preliminary in vitro functional evidence for reflex responses to noxious stimuli in the arms of Octopus vulgaris. *Journal of Experimental Marine Biology and Ecology.* 2013;447:100-105.

27. Andrews PLR, Darmaillacq AS, Dennison N, et al. The identification and management of pain, suffering and distress in cephalopods, including anaesthesia, analgesia and humane killing. *Journal of Experimental Marine Biology and Ecology.* 2013;447:46-64.

28. Kiessling F, Pichler BJ, Hauff P. *Small Animal Imaging: Basics and Practical Guide*: Springer International Publishing; 2017.

29. Fossati SM, Carella F, De Vico G, et al. Octopus arm regeneration: role of Acetylcholine Esterase during morphological modification. *Journal of Experimental Marine Biology and Ecology.* 2013;447:93-99.

30. Novicki A, Messenger J, Budelmann B, et al. [14C]deoxyglucose Labelling of Functional Activity in the Cephalopod Central Nervous System. *Proceedings: Biological Sciences.* 1992 249:77-82.

31. Thabrew MI, Poat PC, Munday KA. Carbohydrate metabolism in Carcinus maenas gill tissue. *Comp Biochem Physiol* 1971;40B: 531-541.

32. Storey KB, Storey JM. Octopine metabolism in the cuttlefish, Sepia officinalis- octopine production by muscle and its role as an aerobic substrate for non-muscular tissues. *J Comp Physiol* 1979;131:311–319.

33. Hochachka PW, Fields JHA. Arginine, glutamate, and proline as substrates for oxidation and for glycogenesis in cephalopod tissues. *Pac Sci.* 1982;36:325-335.

34. Garlick PJ, McNurlan MA, Preedy VR. A rapid and convenient technique for measuring the rate of protein synthesis in tissues by injection of3H phenylalanine. *Biochem J.* 1980;192:719–723.

35. Houlihan DE, McMillan D.N., Agnisola C, et al. Protein synthesis and growth in Octopus vulgaris. *Mar Biol* 1990;106:251-259.

36. Bertetti C. Contributo alla conoscenza del sistema vascolare nei cefalopodi. *Rend Accad nazl XL ser 4.* 1956;6-7.

37. Hill RB, Welsh JH. Heart, Circulation, and Blood Cells. In: Wilbur KM, Yonge CM, eds. *Physiology of Mollusca.* Vol II. New York: Academic press; 1966.

38. O'Dor RK, Wells MJ. Circulation time, blood reserves and extracellular space in a cephalopod. *J Exp Biol.* 1984;113:461-464.

39. Storey KB, Storey JM, Johansen K, et al. Octopine metabolism in Sepia officinalis- Effect of hypoxia and metabolite loads on the blood-levels of octopine and related-compounds. *Can J Zool* 1979;57:2331–2336.

40. Goddard C, Martin A. Carbohydrate metabolism. In: Wilbur KaY, C., ed. *Physiology of Mollusca.* Vol 2: Academic Press; 1966:275-308.

41. Fossati SM, Carella F, Benfenati F, et al. Octopus arm regeneration and its potential implication in reparative pathways. *Journal of Shellfish Research.* 2011;30:1003.

42. Cory HT, Rose SPR. Glucose and amino acid metabolism in octopus optic and vertical lobes in vitro. *J Neurochem.* 1969;16:979–988.

43. Zammit VA, & Newsholme, E. A. The maximum activities of hexokinase, phosphorylase, phosphofructokinase, glycerol phosphate dehydrogenases, lactate dehydrogenase, octopine dehydrogenase, phosphoenolpyruvate carboxykinase, nucleoside diphosphatekinase, glutamate-oxaloacetate transaminase and arginine kinase in relation to carbohydrate utilization in muscles from marine invertebrates. *Biochemical Journal.* 1976;160:447–462.

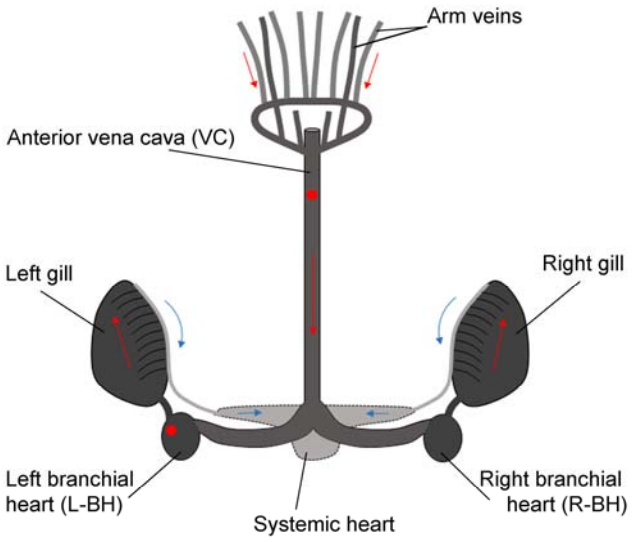

FIGURE.1 Schematic representation the injection locations into the octopus venous system used in this study. Red dots label the two injection locations, these are both upstream the redistribution of the blood to the organs (L-BH: Left branchial heart; VC: anterior vena cava). For clarity, the systemic heart is also shown. Red and blue arrows indicate respectively the main direction followed by the blood return flow and by the oxygenated blood in the hearts and gills. L-BH: left branchial heart, R-BH: right branchial heart, VC: anterior vena cava

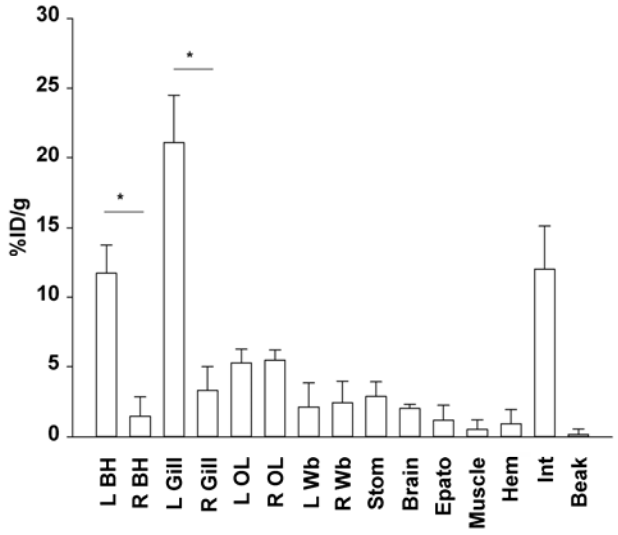

FIGURE.2 γ-counting analysis of ^{18}F-FDG uptake in L-BH animals.

γ-counts of selected organs after L-BH injection are plotted as mean and SE. Data are expressed as percentages of injected dose per gram (%ID/g; n=3). Left branchial hearts (L BH) and gills (L Gill) showed the highest uptake (*t*-test, *P<0.05). Organs farther from the administration site did not show sign of lateralization (ANOVA, Kruskal-Wallis, P>0.05; n=3); Epato: epatopancreas, Hem: hemolymph, Int: intestine, L BH: left branchial heart, L Gill: left gill, L OL: left optic lobe, L Wb: left white body, R BH: right branchial heart, R Gill: right gill, R OL: right optic lobe, R Wb: right white body; Stom: stomach

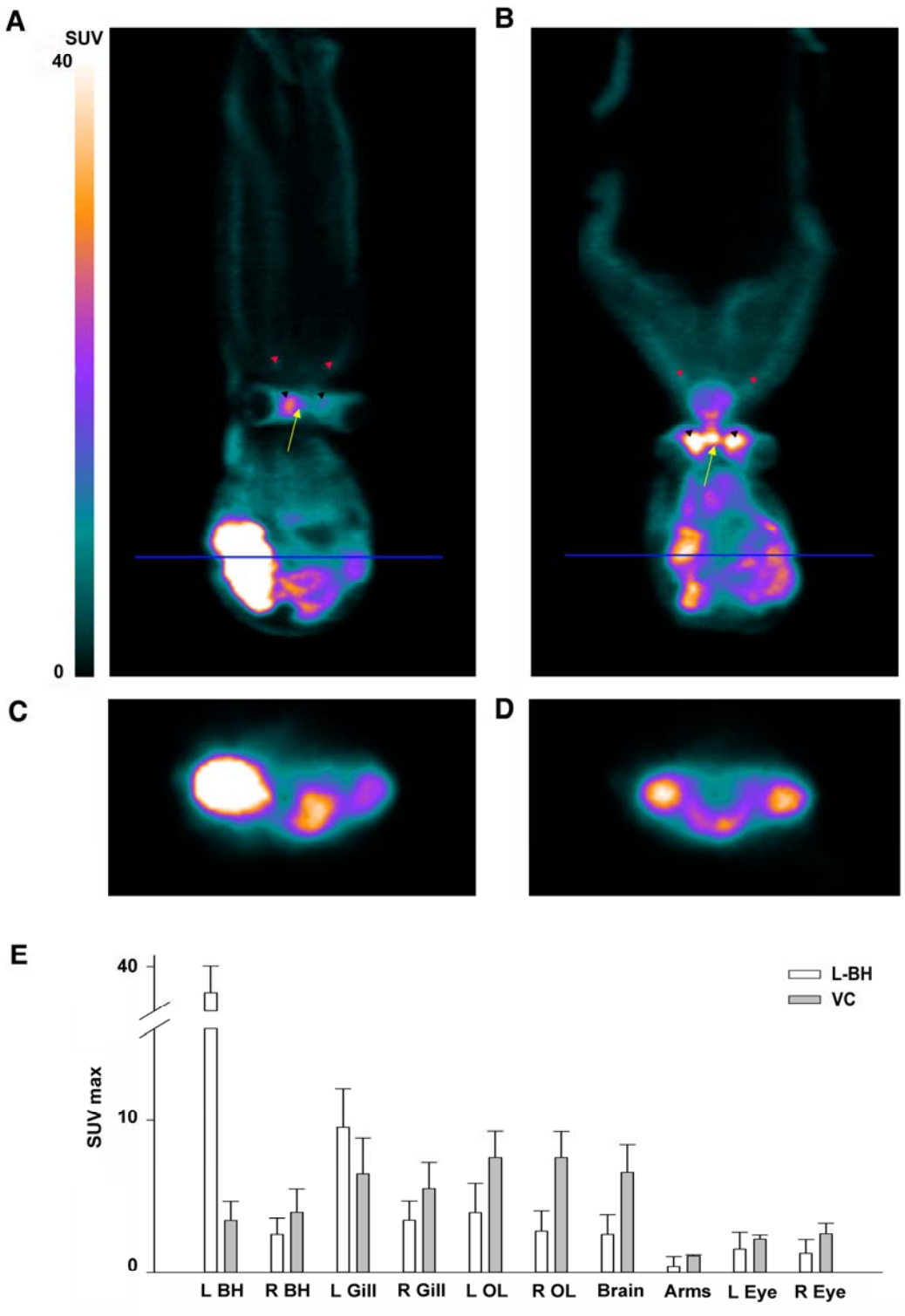

FIGURE.3 ^{18}F-FDG micro-PET images of L-BH and VC animals.

A,B. High metabolic active body regions accumulate vast amounts of 18F-FDG in both L-BH (**A**) and VC (**B**) animals. Yellow arrows point at the central brain; black arrowheads denote optic lobes and red

arrowheads point to the arms. **C,D.** Accumulation at the branchial heart site is evident in L-BH animal (**C**), as compared to VC animal (**D**). **E.** SUV_{max} values in L-BH (n=3) and VC animals (n=2) in the selected organs. Data are plotted as mean and SE. L BH: left branchial heart, L-BH: left branchial heart injected animals, L Eye: left eye, L Gill: left gill, L OL: left optic lobe, R BH: right branchial heart, R Eye: right eye, R Gill: right gill, R OL: right optic lobe, VC: vena cava injected animals

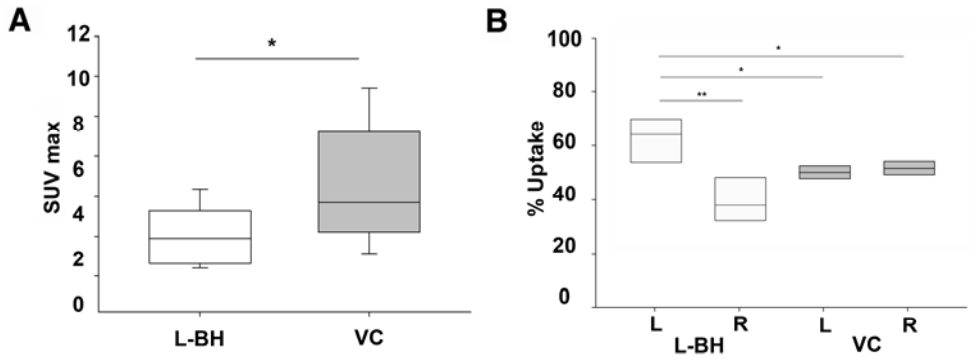

FIGURE.4 Comparison of SUV measures in L-BH and VC animals.

A. Box plots demonstrating the lower uptake in L-BH organs vs VC animals (Mann-Whitney Rank Sum Test, *P<0.05; n=5). **B.** L-BH animals show a significantly higher uptake on the left side (L) than on right side (R) (*t*-test, **P<0.01; n=5). %Uptake of L in L-BH animals was also higher than L and R of VC animals (*t*-test, *P<0.05; n=5). Values are reported as percentages of the total uptake in the L and R organs selected; median values are shown as black bars. L-BH: left branchial heart injected animals, L: left side, R: right side, VC: vena cava injected animals

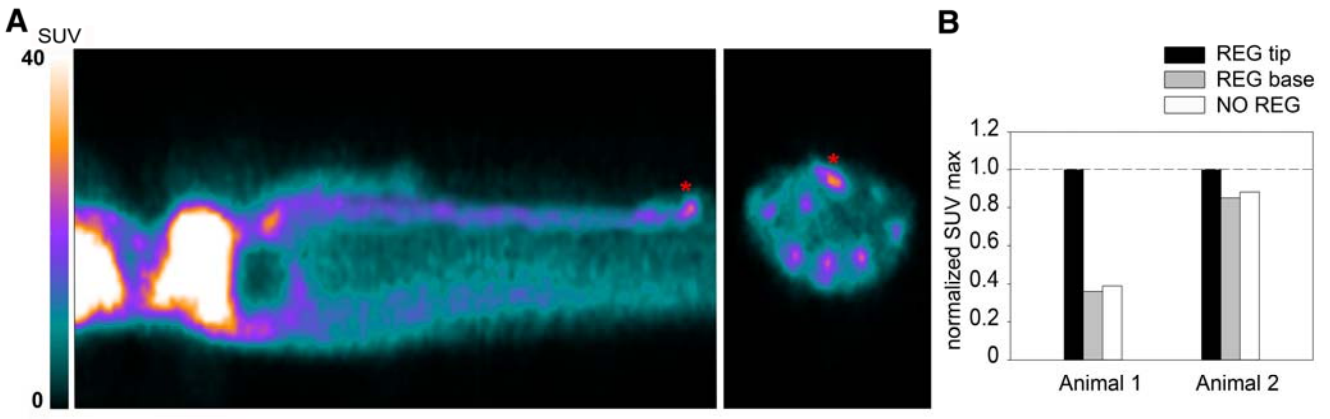

FIGURE.5 ^{18}F-FDG uptake in regenerating arms.

A. micro-PET image of Animal 1 carrying the first left arm at 11 days of regeneration (red asterisks). **B.** FDG uptake measured in the arms of two animals carrying one regenerating arm each (L1) respectively at 11 (Animal 1) and 33 days of regeneration (Animal 2). SUV_{max} values in normal non-regenerating arms (NO REG) and in regenerating arm tip (REG tip) and base (REG base) are reported after normalization to the maximum arm uptake for each animal. REG: regenerating

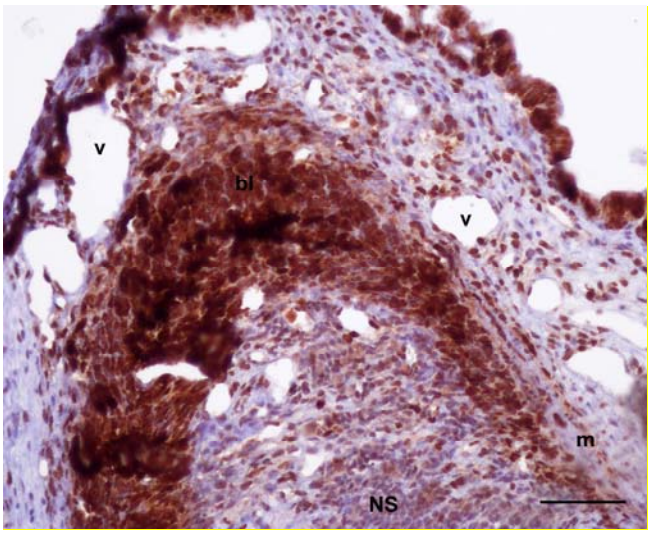

FIGURE.6 Histological section of a regenerating arm tip.

The tip of a regenerating arm at day 17 shows a high proliferation rate (represented by brown precipitation after PCNA reaction) in particular at the region of the blastema (bl) and at both the nervous (NS) and muscular system (m). Vascular components (v) are also present and cover a proximo-distal area of up 1 mm from the arm tip (scale bar 100µm). blastemal: bl, m: muscular system, NS: nervous system, v: vascular components